ACS APPLIED MATERIALS & INTERFACES

www.acsami.org

Research Article

Flexible Piezoresistive Sensors with Wide-Range Pressure Measurements Based on a Graded Nest-like Architecture

Xiao Guan, Ziya Wang,* Wenyu Zhao, Huayi Huang, Shaoping Wang, Qi Zhang, Dongxia Zhong, Waner Lin, Ning Ding,* and Zhengchun Peng*

Cite This: *ACS Appl. Mater. Interfaces* 2020, 12, 26137−26144

Read Online

ACCESS | Metrics & More | Article Recommendations | Supporting Information

ABSTRACT: Flexible pressure sensors present great potential in the application of human health monitoring, tactile function of prosthesis, and electronic skin for robotics. These applications require different trade-off between the sensitivity and sensing range, therefore, it is imperative to develop range-specific sensitivities in a single sensor. In this paper, a bioinspired strategy for a resistive pressure sensor using a graded porous material is proposed to measure pressures from several pascals to megapascals. Its fabrication is based on an easily accessible template method. The nest-architecture-based wide-range pressure sensor exhibits adequate sensitivity under an extensive pressure regime (20 Pa to 1.2 MPa). In addition, with rational structural design and subtle engineering of the material properties, the sensor achieves remarkable mechanical stability. To prove the concept, sensors were attached on a bicycle wheel to monitor the tire-pavement pressure and on human skin to detect biosignals such as venous and arterial blood pressure pulses.

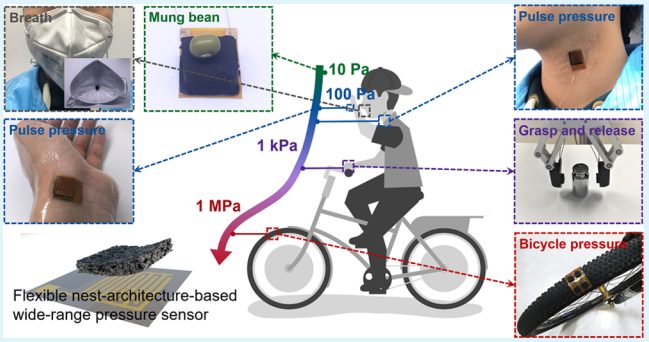

KEYWORDS: *flexible pressure sensor, piezoresistive elastomer, graded nest architecture, wide-range pressure sensing, electronic skins*

INTRODUCTION

In the last decade, flexible pressure sensors have received significant attention from both academic and industrial researchers because of their potential application in wearable electronics[1−4] and robotic tactile sensing.[5,6] Piezoresistive sensors, which have inherently low energy consumption, straightforward read-out connections, a broad pressure detection range, and facile and scalable fabrication processes,[7,8] are finding wide applications in health monitoring devices,[9] electronic skin,[10,11] and intelligent robotics.[12] As new applications such as these emerge, conventional piezoresistive pressure sensors, having an active layer of a planar elastomer composite incorporating conductive materials, are required to have new performance characteristics. In order to meet the needs of more applications, these sensors are expected to detect subtle pressure stimuli with high sensitivity while also having a working range extending to high pressures.[13]

In general, there are two response mechanisms of piezoresistive pressure sensors under external loads: the change of contact resistance between the functional film (or an interlocked micro-/nanoscale structured film) and the counter electrodes and the conductivity change of the sensing material itself.[14] A variety of topographical microstructures such as pillars,[15] hemispheres,[16] triangular pyramids,[7] and interlocked microstructures[17,18] have been used in the structural design of flexible piezoresistive sensors to improve their sensitivity, detection limit, and response time. Generally, these functional materials and substrates with a unique microstructure can indeed effectively improve the sensitivity and detection limit of the sensor.[14,19,20] However, both natural and artificial micro/nanostructured flexible objects cannot maintain high sensitivity under high pressure (>100 kPa).[21,22] The main reason is the contact area of these micro/nanostructured sensors is easily saturated under relatively low pressures.[23] A piezoresistive three-dimensional (3D) monolithic conductive sponge, which can be fabricated by coating in a freeze-drying assembly and direct synthesis with conductive nanomaterials, is limited by residual deformation after being subjected to high pressures. This results from the materials' intrinsically rigid and fragile nature, as well as the poor adhesion between the conductive material and the sponge.[24,25] Although other sponge-like pressure sensors (such as the template-based, porous reverse micelle-induced, and laser-scribed graphene pressure sensor) can respond to high pressures, they exhibit limited sensitivity.[23,26,27] To summarize,

Received: February 20, 2020
Accepted: May 19, 2020
Published: May 19, 2020

https://dx.doi.org/10.1021/acsami.0c03326
ACS Appl. Mater. Interfaces 2020, 12, 26137−26144

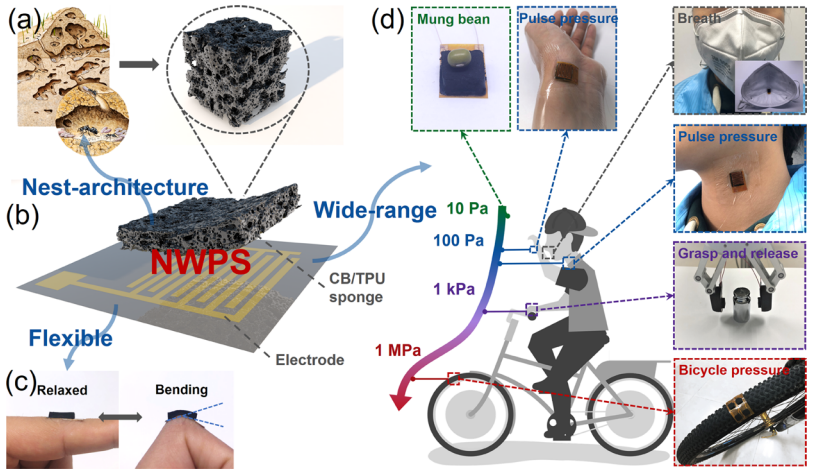

Figure 1. Schematics and applications of the flexible NWPS. (a) Photograph of ant nests. (b) Exploded diagram of the NWPS. (c) Illustration of the NWPS bending with a finger. (d) Various applications exploiting the high sensitivity and wide detection range of the NWPS.

it is challenging to balance the sensitivity and sensing range of the piezoresistive device.[14] Efforts are focused on achieving a wide effective range, from several Pa to MPa pressures, while maintaining high sensitivity.[28] Moreover, expensive ingredients and manufacturing processes hinder the production and use of soft electronics as well.[29−31]

It has been demonstrated that combining rational structural design and materials with subtle properties can achieve high-sensitivity pressure sensors with a wide working range.[8,13] Many insects as nature's architects have shown innate abilities to create remarkable porous structures such as honeycombs, spider webs, and ant nests.[32,33] Investigating the ants' nest in more detail, researchers found that its architecture has a 3D interlaced hierarchical porous structure that has excellent mechanical character to protect the nest from destruction.[34] The hierarchical porous structures offer the maximized contact area and intermolecular interactions and minimized diffusive resistance to both the external stimulus and internal transport by well-defined pore dimensions and topologies compared with the conventional porous structures with uniform pore dimensions. The hierarchical porous structures have been used in sensing, energy, and catalysis because of their unique structural features.[35] To improve the mechanical stability and sensing characteristics of pressure sensors, it is a logical step to exploit the morphologies and structures successfully used in nature by living creatures.

Our flexible piezoresistive sensor based on a graded nest-like architecture is demonstrated to enhance its sensitivity and pressure detection range because of the synergistic effect between the design of the bioinspired nest architecture and carbon black (CB) percolation network. Specifically, it shows an improved sensitivity (1.12 kPa^{-1}), a low detection limit of 20 Pa, and an ultrawide measuring range up to 1.2 MPa. This architecture also contributes to a rapid response time (≈15 ms) and a high stability over 10,000 loading and unloading cycles. Conductive CB nanoparticles are used as the active material because of their distinctive characteristics of sufficient mechanical strength during large pressure loadings,[36] high stability in percolation conductives,[37] and dispersibility in polymer matrixes that is superior to other carbon nanomaterials (e.g., nanofibers, nanosheets, nanotubes, and graphene).[37,38] Moreover, sacrificial particulate templates with tunable sizes are employed to obtain the nest-like architecture inside the polymer composite, which increases the sensitivity to pressure. Finally, echoing the biodesign origins of the device, it has been successfully used to detect physiological signals [wrist and jugular venous pulse (JVP)], as well as in auxiliary robot object manipulation and monitoring the bicycle tire pressure.

METHODS

Device Fabrication. The nest-architecture-based wide-range pressure sensor (NWPS) device was made up of a sensing layer and commercial flexible interdigitated electrodes [flexible printed circuit board (FPCB)]. FPCB was manufactured by the photolithography process and bought from Guangzhou Shentian Electronic Technology Co., Ltd. Figure S1 gives the size information of the interdigital electrode and the effects of the interdigitated electrode geometry on the sensitivity and initial resistance of the NWPS. The slurry of the sensing layer was compounded from commercially available thermoplastic polyurethane (TPU) dissolved in a *N*,*N*-dimethylformamide (DMF) solvent mixed with NaCl particles and CB (SUPER P Li, TIMCAL), which act as a sacrificial template and an electrical conductor, respectively. Before mixing, planetary ball milling (F-P400, FOCUCY) was used to reduce the size of the NaCl particles below 100 μm (540 rpm for 15 min). CB was first dispersed in 20 mL of ethanol (99.5%, Aladdin) under sonication (JY92-IIDN, SCIENTZ) for 10 min and then dried in an oven at 80 °C for 12 h to remove the residual ethanol. After pretreatment, a specific ratio of NaCl, CB, and TPU was uniformly stirred together as a slurry using a double-blade planetary vacuum mixer (HM800, HASAI) for 5 min. The slurry was then transferred into a 3D printed mold, which was made by a fused deposition modeling 3D printer (CR-5, Creality 3D) and fixed onto the FPCB surface. After curing at 80 °C for 4 h, the assembly was immersed in water for 2 h. To ensure that the NaCl particles were removed entirely, the mold was released, and the NWPS device was immersed in water for another 12 h; the water was refreshed every 2 h. Finally, the NWPS device was dried at 80 °C for 2 h.

Characterization of the Hierarchically Porous Architecture. The morphologies and microstructures of the sensing layer were observed using a field emission scanning electron microscope (Supra 55, ZEISS).

Electromechanical Measurements. The NWPS was mounted on a universal material testing machine (E1000, Instron) connected to a digital multimeter (34465A, Keysight) for the real-time monitoring of resistance change. Two NWPSs were fixed on a robot gripper (RG2, OnRobot) mounted on a robot arm (UR5, Universal Robots) which followed the robot gripper to complete the gripping and releasing.

https://dx.doi.org/10.1021/acsami.0c03326
ACS Appl. Mater. Interfaces 2020, 12, 26137−26144

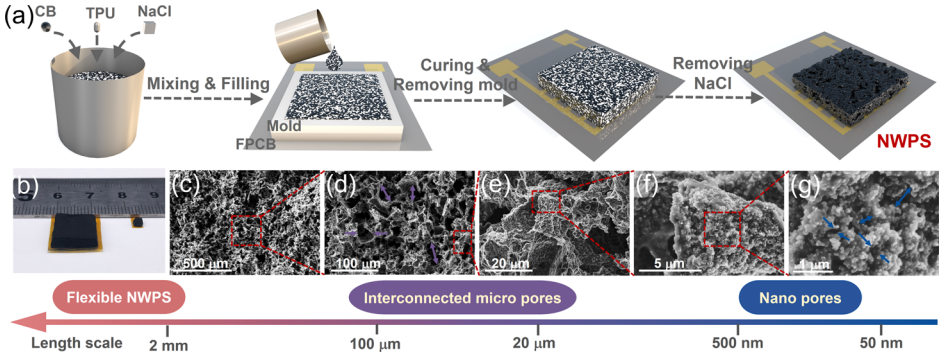

Figure 2. Schematic of the fabrication process flow and hierarchically porous architecture of the flexible NWPS. (a) Fabrication process of the NWPS. (b) Photographic images of the NWPS with volumes of 10 × 10 × 3 mm^3 and 2 × 2 × 3 mm^3. (c–g) SEM images of the 3D hierarchically porous sensing layer at various scales.

RESULTS AND DISCUSSION

A schematic of the flexible NWPS inspired by the hierarchical porous characteristics of the ant nest architecture (Figure 1a) is shown in Figure 1b. Benefiting from the bioinspired hierarchical porous design, our NWPS shows desirable flexibility (Figure 1c) and an ultrawide measuring range with high sensitivity. Its performance makes it suitable for monitoring a wide range of signals from low to high pressures (lightweight common grains or seeds, physiological signals, robotic manipulator force signals, and bicycle tire pressures), as shown in Figure 1d.

The schematic of fabricating the NWPS is shown in Figure 2a. The uniform TPU/CB/NaCl slurry was coated onto the FPCB by a molding method. As a result of the dissolution of DMF in both the TPU matrix and the polyimide matrix of FPCB, the sensing layer and polyimide substrate of FPCB were joined by chemical bonding. After heat treatment and removal of NaCl, the flexible NWPS device was obtained. As shown in Figure 2b, NWPSs with different sizes were prepared by molding, which implies that the NWPS can be customized. The sensing size of the representative device is 10 × 10 × 3 mm^3 in this paper.

The microstructure of the sensing layer was characterized via field emission scanning electron microscopy (FESEM). Similar to the ants' nest architecture, the NWPSs generally have a high porosity and contain a two-hierarchy pore structure with pore sizes varying from the micrometer to nanometer range. As shown in Figure 2c–e, the first level of the hierarchy (larger scale) consists of interconnected pores with a size distribution from 20 to 100 μm, which are left by the dissolution of NaCl. The second level of hierarchy (smaller scale) contains an intrinsic pore size of 50–500 nm (Figure 2f,g), resulting from the densely packed CB nanoparticles around the voids, and they were bonded by TPU. Many exposed CB nanoparticles were found on the surfaces of the pore walls, which is helpful to improving the sensitivity of the NWPS. In this homogeneous porous microstructure with a hierarchy of feature sizes, the contact area between the conductive walls will be increased under pressure loading, resulting in a decrease of both the contact resistances and the channel resistances.[39]

Schematics of the sensing mechanism are shown in Figure 3. R_{total} (total resistance) for a representative path through the material can be defined as[40]

$$R_{total} = R_C + R_P \quad (1)$$

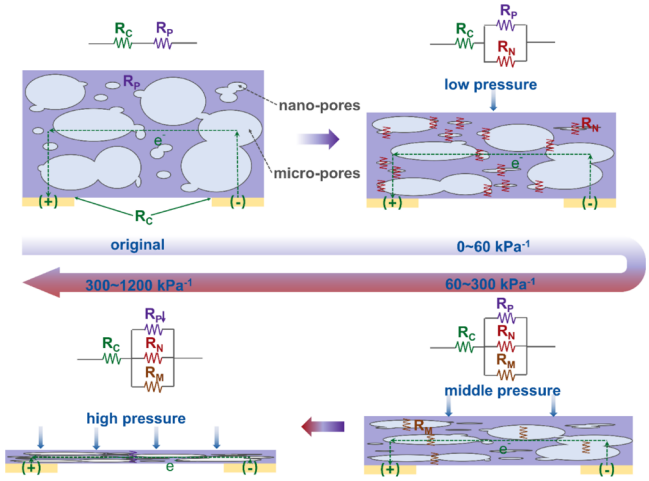

Figure 3. Modeling of the piezoresistive mechanism.

where R_C is the contact resistance between the sensing layer and the FPCB. Because of the excellent combination of the homogeneous polymers at the interface, R_C is virtually unchanged as the pressure increases. The second resistance component, R_P, is the percolation resistance of the hierarchically porous piezoresistive elastomer.

In Figure 3, the nanopores located in the agglomerated CB nanoparticles can be closed easily by elastic deformation at the microscale in the low-pressure regime. These closed nanopores can be modeled as a contact resistance R_N, which is connected in parallel to the R_P, dropping the total resistance.

$$R_{total} = R_C + \frac{R_P \times R_N}{R_P + R_N} \quad (2)$$

Under a middle-pressure loading, R_N and R_P are paralleled by the contact resistance R_M resulting from the closing of the micropores, and the total resistance is further reduced.

$$R_{total} = R_C + \frac{R_P \times R_N \times R_M}{R_P \times R_N + R_P \times R_M + R_N \times R_M} \quad (3)$$

As pressure loading increases even further, severe flattening of the pressure sensor occurs, causing the sensing layer to become a solid film, leading to a significant decrease in the percolation resistance R_P: the total resistance of the sensing layer drops continually. In the ant nest-structured foam with its hierarchical porosity, deformation is hindered by the structural stiffening with increasing pressure, and the NWPS maintains its

https://dx.doi.org/10.1021/acsami.0c03326
ACS Appl. Mater. Interfaces 2020, 12, 26137–26144

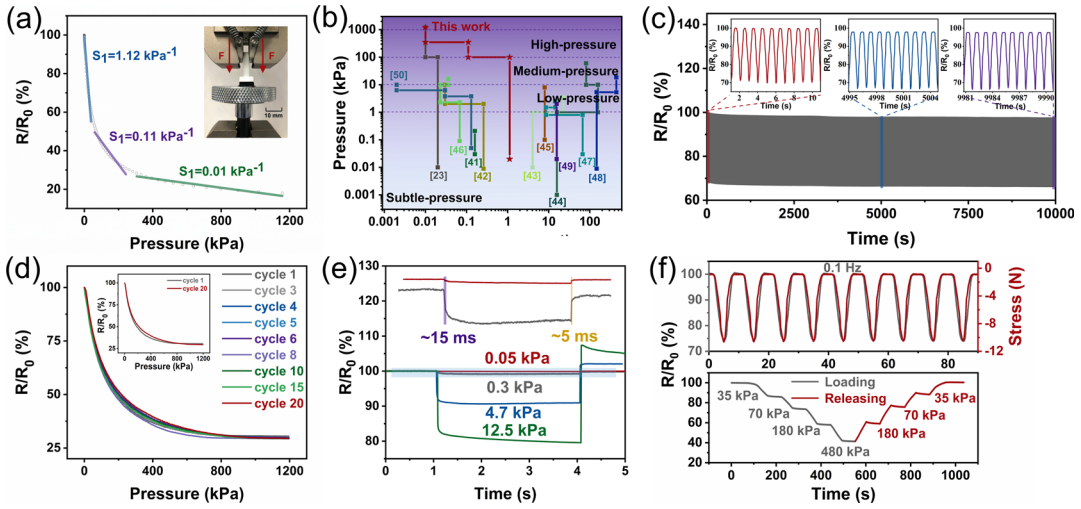

Figure 4. Evaluation of the electromechanical performance of the NWPS. (a) Resistance response of the NWPS vs pressure loading. (b) Comparison of the sensitivity and measuring range between this NWPS and previously reported flexible pressure sensors. (c) 10,000 loading−unloading tests of the NWPS at 1 Hz illustrating the stability and durability. (d) Repeatability measurement. (e) Response (left) and relaxation (right) times at different pressures. (f) Dynamic response of the NWPS at a frequency of 0.1 Hz (upper panel) and under stepped pressures (lower panel).

excellent linear sensing properties through each broad pressure range.

The effects of the NaCl and CB mass ratio on pressure sensitivity and resistivity were studied (Figures S2, Supporting Information). We found that the increased NaCl content decreases the conductivity and elastic modulus of the sponge in its rest state, leading to a decrease in strength and resilience, while the addition of CB produces the opposite effect. To determine the optimal ratio for the highest sensitivity, variables were controlled and the maximum is found when the mass ratio of NaCl and TPU is approximately 5:1 and the mass ratio of CB and TPU is 1:4.

Furthermore, with increased CB nanoparticle content, the initial resistance is modified, the mechanical strength tolerates significant pressure loadings, and the conductive percolation networks are stable against deformation. When the mass ratio is over 25%, the sensitivity of the NWPS decreases as a result of the increased intrinsic conductivity and the reduced elastic modulus. In summary, the mass ratio of TPU/CB/NaCl for the best-performed sensor is 1:0.25:6. The device discussed in the following sections is fabricated at this optimized ratio unless otherwise stated.

The sensitivity (S) generally utilized to evaluate the performance of a resistance-based pressure sensor is defined as

$$S = \frac{\Delta R}{\Delta P \times R_0} \tag{4}$$

where R and P are the resistance of the sensor and the external pressure, respectively. R_0 is the resistance when $P = 0$. ΔP is the pressure change. ΔR is the resistance change of the sensor under ΔP pressure loading. The resistance response curve of the NWPS shows the typical pattern of three linear regions (Figure 4a). The fitted sensitivities are 1.12 kPa^{-1} for the range under the pressure of 60 kPa, 0.11 kPa^{-1} for the range of 60−300 kPa, and 0.01 kPa^{-1} for the range of 300−1200 kPa. The correlation coefficient (R^2) of each linear pressure range is presented in Figures S3 (Supporting Information). In contrast to sensors in the literature,[23,41−50] the NWPS exhibits high sensitivities over a comprehensive pressure range of 20 Pa to 1.2 MPa (Figure 4b). Although some previous pressure sensors reported a higher sensitivity than our sensor, most of them exhibited a limited pressure range (<10 kPa). Except for the NWPS, few sensors can cover all pressure regimes in daily life from subtle contact to high-pressure contact. Furthermore, the NWPS maintains its toughness (no mechanical damage or permanent deformation at 120 N/1.2 MPa) and flexibility simultaneously (the modulus, measured at a compressive strain of 10%, was 77.8 kPa), as exhibited in Figures S4 and S5 and Movie S1 (Supporting Information).

High-mechanical durability is required to maintain a stable input−output relationship of flexible pressure sensors under long-term or cyclic loading. In Figure 4c, the NWPS was tested under a repetitive cyclic pressure load of 30 kPa at 1 Hz. It maintained a reliable and uniform pressure-sensing performance up to 10,000 cycles. To further demonstrate the hysteresis characteristic of the NWPS, a typical loading−unloading cycle is shown in Figure S6a (Supporting Information). This test indicates that the pressure sensing curve during unloading is in good agreement with that of loading, and the response of the sensor returns to the initial point.

Figure 4d shows excellent repeatability of the NWPS; there is little difference between these 20 curves. At different pressures (0.05, 0.3, 4.7, and 12.5 kPa), the NWPS shows fast response and relaxation times of ≈15 and ≈5 ms (Figure 4e), respectively, which are faster than the response time of human skin (30−50 ms). Also, the NWPS returned to its initial state in a short time after the removal of the applied pressure, which shows favorable recoverability. A sinusoidal cyclic loading with 0.1 Hz frequency (Figure 4f, top) and the cyclic loading from low pressure to high pressure (70 Pa to 202 kPa) at 1 Hz (Figure S6b, Supporting Information) were employed. It is observed that the NWPS always responds synchronously and stably during both tests. Because of the viscoelasticity of the polymer, the resistance of the sensor is usually higher than the initial resistance value after the pressure is released, which becomes more evident as the load increases. Further reversibility tests were performed by applying a sequence of step loading to the NWPS (Figure 4f, bottom). The

https://dx.doi.org/10.1021/acsami.0c03326
ACS Appl. Mater. Interfaces 2020, 12, 26137−26144

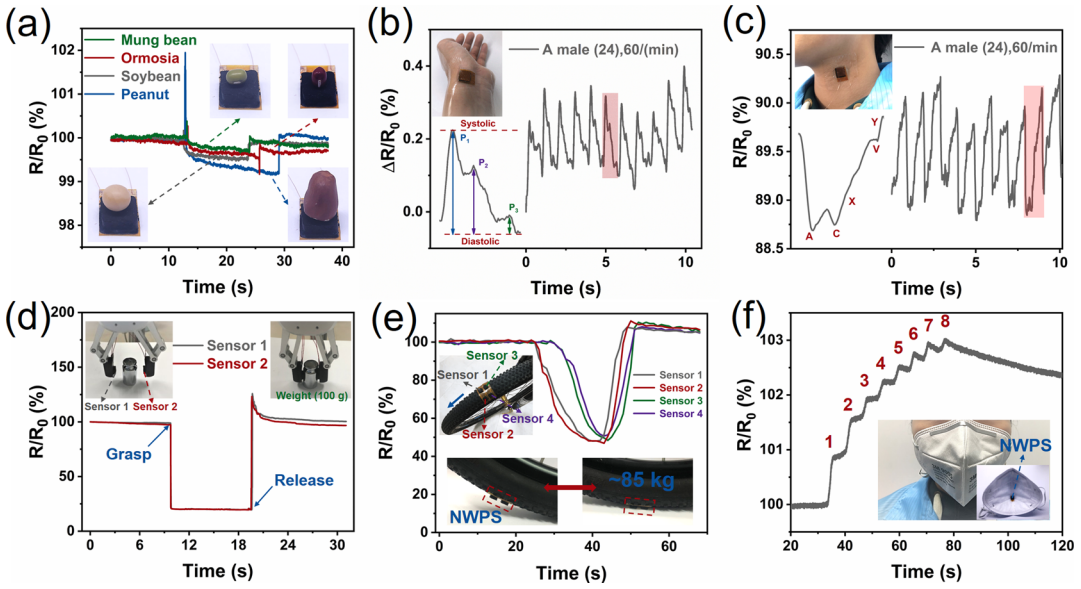

Figure 5. Various applications of the flexible NWPS. (a) Weighing common seeds. (b) Real-time radial artery pulse monitoring. (c) Real-time JVP monitoring. (d) Gripping and releasing a weight by a robotic gripper. (e) Four-channel sensor matrix crushed by the tire of a bicycle (weight of 85 kg). (f) Monitoring human breathing.

corresponding resistance responses demonstrate its outstanding ability to identify absolute pressure. The rationally chosen modulus and viscoelasticity values lead to the high response speed of the NWPS.

Common grains and seeds were used to verify the high sensitivity and the low detection limit of the NWPS. The subtle dynamic information that a mung bean (equivalent pressure ≈ 20 Pa) was gently placed on the sensor and then moved away was captured by the NWPS (Figure 5a). Figure 5b shows real-time monitoring of radial artery pressure pulses (Movie S2, Supporting Information). The flexible NWPS was attached to a volunteer's wrist by 3M medical tape. As can be seen from the recorded signal waveform (illustrated in Figure 5b), the volunteer's wrist pulse rate was about 60 beats per minute. Furthermore, the NWPS can quantitatively distinguish characteristic peaks in the pulse waveform, which contains three distinct peaks: P_1, P_2, and P_3 (percussion wave, tidal wave, and diastolic wave). The calculated radial artery augmentation index ($AI_r = P_2/P_1$) and the radial diastolic augmentation index ($DAI = P_3/P_1$) are 0.60 and 0.15 on average, which matches the reference data of a normal 25 year old man.[51] The deep-lying internal JVP signals in Figure 5c again demonstrate the capability of measuring weak signals with the flexible NWPS. Typically, a distinct biphasic waveform of JVP contains three upward and two downward deflections.[52] These are correlated with the following cardiac mechanisms: the upward deflections are denoted "a" (atrial contraction), "c" (ventricular contraction), and "v" (atrial venous filling); the downward deflections are denoted "x" (atrium relaxation) and "y" descents (ventricle filling). The results indicate that the NWPS is capable of using a wearable diagnostic device for real-time monitoring because of its high sensitivity and low detection limit.

Besides, in order to assist mechanical gripper to obtain the tactile sense (Figure 5d), two NWPSs were affixed to a robotic gripper to detect the pressures applied to the objects in the process of gripping and release. The NWPSs exhibit a rapid and stable signal feedback. Moreover, there is no difference between sensor 1 and sensor 2. For demonstrating the superior toughness and a wide range of dynamic pressure responses of the NWPS, a bicycle tire rollover experiment using a four-channel NWPS matrix was conducted. The profile of the trajectory is clearly recorded in real time in the pressure trace. The motion of the bicycle, moving from sensors 1 and 2 to sensors 3 and 4, is distinguishable in the graph (Figure 5e) showing the resistance signals. Figure 5f demonstrates that the NWPS can also be used to monitor human breathing. This is because the NWPS possesses a positive resistance response to humidity because of swelling of the polymer matrix, which increases the distance between CB particles and hinders the electron transport in the polymer matrix.[53] In addition, the NWPS is able to detect alcohol in human breath and distinguish between different solvents such as deionized water and alcohol as a result of polymer−odorant interactions (Figures S7, Supporting Information).[54]

CONCLUSIONS

In summary, we report a low-cost, flexible pressure sensor with a unique 3D hierarchical porous structure that is inspired by the natural design of ant nests and fabricated using an easily accessible template method. An optimized nest structure and the unique material properties of the sensor contribute to an adequately high sensitivity, a low detection limit of 20 Pa, and an ultrawide measurement range of up to 1.2 MPa. This range covers all pressure regimes found in daily life and also includes some extremely high-pressure cases, which allows the application of our sensor in some extreme environment. Moreover, no costly materials or sophisticated equipment is involved throughout the manufacturing process of the flexible sensor. We successfully demonstrated a variety of the use cases of our sensor, including health parameter detection, biking pressure monitoring, and robotic tactile sensing. We believe that the bioinspired nest structure can provide a general design strategy for other types of sensors as well.

https://dx.doi.org/10.1021/acsami.0c03326
ACS Appl. Mater. Interfaces 2020, 12, 26137−26144

■ ASSOCIATED CONTENT

Supporting Information

The Supporting Information is available free of charge at https://pubs.acs.org/doi/10.1021/acsami.0c03326.

Size information of the interdigital electrode and the effects of the interdigitated electrode geometry on the sensitivity and initial resistance of the NWPS; effects of the NaCl and CB mass ratio on the resistivity and sensitivity of the NWPS; correlation coefficient of each linear pressure range; excellent toughness of the NWPS; compressive stress−strain curves of the NWPS; hysteresis characteristics and dynamic response under cyclic loading from low pressure to high pressure (70 Pa−202 kPa) at a frequency of 1 Hz of the NWPS; detecting alcohol in human breath and distinguishing between different solvents; and four-channel NWPS data acquisition systems (PDF)

NWPS still retaining its original state after applying a 120 N force (MP4)

Monitoring of pulse signals (MP4)

■ AUTHOR INFORMATION

Corresponding Authors

Ziya Wang − *Shenzhen Institute of Artificial Intelligence and Robotics for Society (AIRS), Shenzhen 518129, P. R. China;* orcid.org/0000-0002-9582-8139; Email: wzywolf@163.com

Ning Ding − *Institute of Robotics and Intelligent Manufacturing (IRIM), The Chinese University of Hong Kong, Shenzhen 518172, P. R. China*; Email: dingning@cuhk.edu.cn

Zhengchun Peng − *Center for Stretchable Electronics and Nano Sensors (SENS), Key Laboratory of Optoelectronic Devices and Systems of Ministry of Education, College of Physics and Optoelectronic Engineering, Shenzhen University, Shenzhen 518060, P. R. China;* orcid.org/0000-0002-7114-1797; Email: zcpeng@szu.edu.cn

Authors

Xiao Guan − *Center for Stretchable Electronics and Nano Sensors (SENS), Key Laboratory of Optoelectronic Devices and Systems of Ministry of Education, College of Physics and Optoelectronic Engineering, Shenzhen University, Shenzhen 518060, P. R. China*

Wenyu Zhao − *Shenzhen Institute of Artificial Intelligence and Robotics for Society (AIRS), Shenzhen 518129, P. R. China*

Huayi Huang − *Center for Stretchable Electronics and Nano Sensors (SENS), Key Laboratory of Optoelectronic Devices and Systems of Ministry of Education, College of Physics and Optoelectronic Engineering, Shenzhen University, Shenzhen 518060, P. R. China*

Shaoping Wang − *Center for Stretchable Electronics and Nano Sensors (SENS), Key Laboratory of Optoelectronic Devices and Systems of Ministry of Education, College of Physics and Optoelectronic Engineering, Shenzhen University, Shenzhen 518060, P. R. China*

Qi Zhang − *Center for Stretchable Electronics and Nano Sensors (SENS), Key Laboratory of Optoelectronic Devices and Systems of Ministry of Education, College of Physics and Optoelectronic Engineering, Shenzhen University, Shenzhen 518060, P. R. China*

Dongxia Zhong − *Center for Stretchable Electronics and Nano Sensors (SENS), Key Laboratory of Optoelectronic Devices and Systems of Ministry of Education, College of Physics and Optoelectronic Engineering, Shenzhen University, Shenzhen 518060, P. R. China*

Waner Lin − *Center for Stretchable Electronics and Nano Sensors (SENS), Key Laboratory of Optoelectronic Devices and Systems of Ministry of Education, College of Physics and Optoelectronic Engineering, Shenzhen University, Shenzhen 518060, P. R. China*

Complete contact information is available at: https://pubs.acs.org/10.1021/acsami.0c03326

Author Contributions

The manuscript was written through contributions of all authors. All authors have given approval to the final version of the manuscript.

Notes

The authors declare no competing financial interest.

■ ACKNOWLEDGMENTS

This work was supported by the Shenzhen Science and Technology Program (KQTD20170810105439418, JCYJ20170818091233245, and JCYJ20170410171923840), the National Natural Science Foundation of China (61903317, 61671308, U1613227, and U1813216), the National Key Research and Development Project (2019YFB1310403), and the Department of Education of Guangdong Province (2016KZDXM005), and funding was provided by the Shenzhen Institute of Artificial Intelligence and Robotics for Society.

■ REFERENCES

(1) Chortos, A.; Liu, J.; Bao, Z. Pursuing prosthetic electronic skin. *Nat. Mater.* **2016**, *15*, 937−950.

(2) Wang, S.; Xu, J.; Wang, W.; Wang, G.-J. N.; Rastak, R.; Molina-Lopez, F.; Chung, J. W.; Niu, S.; Feig, V. R.; Lopez, J.; Lei, T.; Kwon, S.-K.; Kim, Y.; Foudeh, A. M.; Ehrlich, A.; Gasperini, A.; Yun, Y.; Murmann, B.; Tok, J. B.-H.; Bao, Z. Skin electronics from scalable fabrication of an intrinsically stretchable transistor array. *Nature* **2018**, *555*, 83−88.

(3) Sim, K.; Rao, Z.; Zou, Z.; Ershad, F.; Lei, J.; Thukral, A.; Chen, J.; Huang, Q.-A.; Xiao, J.; Yu, C. Metal oxide semiconductor nanomembrane-based soft unnoticeable multifunctional electronics for wearable human-machine interfaces. *Sci. Adv.* **2019**, *5*, No. eaav9653.

(4) Sim, K.; Rao, Z.; Kim, H.-J.; Thukral, A.; Shim, H.; Yu, C. Fully rubbery integrated electronics from high effective mobility intrinsically stretchable semiconductors. *Sci. Adv.* **2019**, *5*, No. eaav5749.

(5) Boutry, C. M.; Negre, M.; Jorda, M.; Vardoulis, O.; Chortos, A.; Khatib, O.; Bao, Z. A hierarchically patterned, bioinspired e-skin able to detect the direction of applied pressure for robotics. *Sci. Robot.* **2018**, *3*, No. eaau6914.

(6) Kim, H.-J.; Sim, K.; Thukral, A.; Yu, C. Rubbery electronics and sensors from intrinsically stretchable elastomeric composites of semiconductors and conductors. *Sci. Adv.* **2017**, *3*, No. e1701114.

(7) Choong, C.-L.; Shim, M.-B.; Lee, B.-S.; Jeon, S.; Ko, D.-S.; Kang, T.-H.; Bae, J.; Lee, S. H.; Byun, K.-E.; Im, J.; Jeong, Y. J.; Park, C. E.; Park, J.-J.; Chung, U.-I. Highly Stretchable Resistive Pressure Sensors Using a Conductive Elastomeric Composite on a Micropyramid Array. *Adv. Mater.* **2014**, *26*, 3451−3458.

(8) Wang, Z.; Guan, X.; Huang, H.; Wang, H.; Lin, W.; Peng, Z. Full 3D Printing of Stretchable Piezoresistive Sensor with Hierarchical Porosity and Multimodulus Architecture. *Adv. Funct. Mater.* **2019**, *29*, 1807569.

(9) Trung, T. Q.; Lee, N.-E. Flexible and Stretchable Physical Sensor Integrated Platforms for Wearable Human-Activity Monitoringand Personal Healthcare. *Adv. Mater.* **2016**, *28*, 4338−4372.
(10) Wang, X.; Dong, L.; Zhang, H.; Yu, R.; Pan, C.; Wang, Z. L. Recent Progress in Electronic Skin. *Adv. Sci.* **2015**, *2*, 1500169.
(11) Sundaram, S.; Kellnhofer, P.; Li, Y.; Zhu, J.-Y.; Torralba, A.; Matusik, W. Learning the signatures of the human grasp using a scalable tactile glove. *Nature* **2019**, *569*, 698−702.
(12) Osborn, L. E.; Dragomir, A.; Betthauser, J. L.; Hunt, C. L.; Nguyen, H. H.; Kaliki, R. R.; Thakor, N. V. Prosthesis with neuromorphic multilayered e-dermis perceives touch and pain. *Sci. Robot.* **2018**, *3*, No. eaat3818.
(13) Lee, Y.; Park, J.; Cho, S.; Shin, Y.-E.; Lee, H.; Kim, J.; Myoung, J.; Cho, S.; Kang, S.; Baig, C.; Ko, H. Flexible Ferroelectric Sensors with Ultrahigh Pressure Sensitivity and Linear Response over Exceptionally Broad Pressure Range. *ACS Nano* **2018**, *12*, 4045−4054.
(14) Tang, X.; Wu, C.; Gan, L.; Zhang, T.; Zhou, T.; Huang, J.; Wang, H.; Xie, C.; Zeng, D. Multilevel Microstructured Flexible Pressure Sensors with Ultrahigh Sensitivity and Ultrawide Pressure Range for Versatile Electronic Skins. *Small* **2019**, *15*, 1804559.
(15) Park, H.; Jeong, Y. R.; Yun, J.; Hong, S. Y.; Jin, S.; Lee, S.-J.; Zi, G.; Ha, J. S. Stretchable Array of Highly Sensitive Pressure Sensors Consisting of Polyaniline Nanofibers and Au-Coated Polydimethylsiloxane Micropillars. *ACS Nano* **2015**, *9*, 9974−9985.
(16) Park, J.; Lee, Y.; Hong, J.; Ha, M.; Jung, Y.-D.; Lim, H.; Kim, S. Y.; Ko, H. Giant Tunneling Piezoresistance of Composite Elastomers with Interlocked Microdome Arrays for Ultrasensitive and Multimodal Electronic Skins. *ACS Nano* **2014**, *8*, 4689−4697.
(17) Pang, C.; Lee, G.-Y.; Kim, T.-i.; Kim, S. M.; Kim, H. N.; Ahn, S.-H.; Suh, K.-Y. A flexible and highly sensitive strain-gauge sensor using reversible interlocking of nanofibres. *Nat. Mater.* **2012**, *11*, 795−801.
(18) Wang, K.; Lou, Z.; Wang, L.; Zhao, L.; Zhao, S.; Wang, D.; Han, W.; Jiang, K.; Shen, G. Bioinspired Interlocked Structure-Induced High Deformability for Two-Dimensional Titanium Carbide (MXene)/Natural Microcapsule-Based Flexible Pressure Sensors. *ACS Nano* **2019**, *13*, 9139−9147.
(19) Pang, Y.; Zhang, K.; Yang, Z.; Jiang, S.; Ju, Z.; Li, Y.; Wang, X.; Wang, D.; Jian, M.; Zhang, Y.; Liang, R.; Tian, H.; Yang, Y.; Ren, T.-L. Epidermis Microstructure Inspired Graphene Pressure Sensor with Random Distributed Spinosum for High Sensitivity and Large Linearity. *ACS Nano* **2018**, *12*, 2346−2354.
(20) Sun, Q.-J.; Zhuang, J.; Venkatesh, S.; Zhou, Y.; Han, S.-T.; Wu, W.; Kong, K.-W.; Li, W.-J.; Chen, X.; Li, R. K. Y.; Roy, V. A. L. Highly Sensitive and Ultrastable Skin Sensors for Biopressure and Bioforce Measurements Based on Hierarchical Microstructures. *ACS Appl. Mater. Interfaces* **2018**, *10*, 4086−4094.
(21) Su, B.; Gong, S.; Ma, Z.; Yap, L. W.; Cheng, W. Mimosa-Inspired Design of a Flexible Pressure Sensor with Touch Sensitivity. *Small* **2015**, *11*, 1886−1891.
(22) Wang, X.; Gu, Y.; Xiong, Z.; Cui, Z.; Zhang, T. Silk-Molded Flexible, Ultrasensitive, and Highly Stable Electronic Skin for Monitoring Human Physiological Signals. *Adv. Mater.* **2014**, *26*, 1336−1342.
(23) Kim, S.; Amjadi, M.; Lee, T.-I.; Jeong, Y.; Kwon, D.; Kim, M. S.; Kim, K.; Kim, T.-S.; Oh, Y. S.; Park, I. Wearable, Ultrawide-Range, and Bending-Insensitive Pressure Sensor Based on Carbon Nanotube Network-Coated Porous Elastomer Sponges for Human Interface and Healthcare Devices. *ACS Appl. Mater. Interfaces* **2019**, *11*, 23639−23648.
(24) Zhuo, H.; Hu, Y.; Tong, X.; Chen, Z.; Zhong, L.; Lai, H.; Liu, L.; Jing, S.; Liu, Q.; Liu, C.; Peng, X.; Sun, R. A Supercompressible, Elastic, and Bendable Carbon Aerogel with Ultrasensitive Detection Limits for Compression Strain, Pressure, and Bending Angle. *Adv. Mater.* **2018**, *30*, 1706705.
(25) Ding, Y.; Yang, J.; Tolle, C. R.; Zhu, Z. Flexible and Compressible PEDOT:PSS@Melamine Conductive Sponge Prepared via One-Step Dip Coating as Piezoresistive Pressure Sensor for Human Motion Detection. *ACS Appl. Mater. Interfaces* **2018**, *10*, 16077−16086.
(26) Tian, H.; Shu, Y.; Wang, X.-F.; Mohammad, M. A.; Bie, Z.; Xie, Q.-Y.; Li, C.; Mi, W.-T.; Yang, Y.; Ren, T.-L. A Graphene-Based Resistive Pressure Sensor with Record-High Sensitivity in a Wide Pressure Range. *Sci. Rep.* **2015**, *5*, 8603.
(27) Jung, S.; Kim, J. H.; Kim, J.; Choi, S.; Lee, J.; Park, I.; Hyeon, T.; Kim, D.-H. Reverse-Micelle-Induced Porous Pressure-Sensitive Rubber for Wearable Human-Machine Interfaces. *Adv. Mater.* **2014**, *26*, 4825−4830.
(28) Jiang, S.; Yu, J.; Xiao, Y.; Zhu, Y.; Zhang, W. Ultrawide Sensing Range and Highly Sensitive Flexible Pressure Sensor Based on a Percolative Thin Film with a Knoll-like Microstructured Surface. *ACS Appl. Mater. Interfaces* **2019**, *11*, 20500−20508.
(29) Park, J.; Lee, Y.; Hong, J.; Lee, Y.; Ha, M.; Jung, Y.; Lim, H.; Kim, S. Y.; Ko, H. Tactile-Direction-Sensitive and Stretchable Electronic Skins Based on Human-Skin-Inspired Interlocked Microstructures. *ACS Nano* **2014**, *8*, 12020−12029.
(30) Guo, S.-Z.; Qiu, K.; Meng, F.; Park, S. H.; McAlpine, M. C. 3D Printed Stretchable Tactile Sensors. *Adv. Mater.* **2017**, *29*, 1701218.
(31) Kim, H.-J.; Thukral, A.; Yu, C. Highly Sensitive and Very Stretchable Strain Sensor Based on a Rubbery Semiconductor. *ACS Appl. Mater. Interfaces* **2018**, *10*, 5000−5006.
(32) Wegst, U. G. K.; Bai, H.; Saiz, E.; Tomsia, A. P.; Ritchie, R. O. Bioinspired structural materials. *Nat. Mater.* **2015**, *14*, 23−36.
(33) Zhao, N.; Wang, Z.; Cai, C.; Shen, H.; Liang, F.; Wang, D.; Wang, C.; Zhu, T.; Guo, J.; Wang, Y.; Liu, X.; Duan, C.; Wang, H.; Mao, Y.; Jia, X.; Dong, H.; Zhang, X.; Xu, J. Bioinspired Materials: from Low to High Dimensional Structure. *Adv. Mater.* **2014**, *26*, 6994−7017.
(34) Qu, W.; Zhou, W.; Zhu, P.; Zhang, Z. Model of Underground Ant Nest Structure Using Static and Dynamic Finite Element Analysis. *Acta Mech. Solida Sin.* **2018**, *31*, 717−730.
(35) Dutta, S.; Bhaumik, A.; Wu, K. C.-W. Hierarchically porous carbon derived from polymers and biomass: effect of interconnected pores on energy applications. *Energy Environ. Sci.* **2014**, *7*, 3574−3592.
(36) Deng, H.; Zhang, R.; Bilotti, E.; Loos, J.; Peijs, T. Conductive polymer tape containing highly oriented carbon nanofillers. *J. Appl. Polym. Sci.* **2009**, *113*, 742−751.
(37) Appel, A.-K.; Thomann, R.; Mülhaupt, R. Polyurethane nanocomposites prepared from solvent-free stable dispersions of functionalized graphene nanosheets in polyols. *Polymer* **2012**, *53*, 4931−4939.
(38) Ding, T.; Wang, L.; Wang, P. Changes in electrical resistance of carbon-black-filled silicone rubber composite during compression. *J. Polym. Sci., Part B: Polym. Phys.* **2007**, *45*, 2700−2706.
(39) Amjadi, M.; Pichitpajongkit, A.; Lee, S.; Ryu, S.; Park, I. Highly Stretchable and Sensitive Strain Sensor Based on Silver Nanowire-Elastomer Nanocomposite. *ACS Nano* **2014**, *8*, 5154−5163.
(40) Zang, Y.; Zhang, F.; Di, C.-a.; Zhu, D. Advances of flexible pressure sensors toward artificial intelligence and health care applications. *Mater. Horiz.* **2015**, *2*, 140−156.
(41) Xu, X.; Wang, R.; Nie, P.; Cheng, Y.; Lu, X.; Shi, L.; Sun, J. Copper Nanowire-Based Aerogel with Tunable Pore Structure and Its Application as Flexible Pressure Sensor. *ACS Appl. Mater. Interfaces* **2017**, *9*, 14273−14280.
(42) Yao, H.-B.; Ge, J.; Wang, C.-F.; Wang, X.; Hu, W.; Zheng, Z.-J.; Ni, Y.; Yu, S.-H. A Flexible and Highly Pressure-Sensitive Graphene-Polyurethane Sponge Based on Fractured Microstructure Design. *Adv. Mater.* **2013**, *25*, 6692−6698.
(43) Ma, Y.; Yue, Y.; Zhang, H.; Cheng, F.; Zhao, W.; Rao, J.; Luo, S.; Wang, J.; Jiang, X.; Liu, Z.; Liu, N.; Gao, Y. 3D Synergistical MXene/Reduced Graphene Oxide Aerogel for a Piezoresistive Sensor. *ACS Nano* **2018**, *12*, 3209−3216.
(44) Wang, Y.; Chao, M.; Wan, P.; Zhang, L. A wearable breathable pressure sensor from metal-organic framework derived nanocomposites for highly sensitive broad-range healthcare monitoring. *Nano Energy* **2020**, *70*, 104560.

https://dx.doi.org/10.1021/acsami.0c03326
ACS Appl. Mater. Interfaces 2020, 12, 26137−26144

(45) Sencadas, V.; Tawk, C.; Alici, G. Environmentally Friendly and Biodegradable Ultrasensitive Piezoresistive Sensors for Wearable Electronics Applications. *ACS Appl. Mater. Interfaces* **2020**, *12*, 8761−8772.
(46) Wu, X.; Han, Y.; Zhang, X.; Zhou, Z.; Lu, C. Large-Area Compliant, Low-Cost, and Versatile Pressure-Sensing Platform Based on Microcrack-Designed Carbon Black@Polyurethane Sponge for Human-Machine Interfacing. *Adv. Funct. Mater.* **2016**, *26*, 6246−6256.
(47) Xiao, J.; Tan, Y.; Song, Y.; Zheng, Q. A flyweight and superelastic graphene aerogel as a high-capacity adsorbent and highly sensitive pressure sensor. *J. Mater. Chem. A* **2018**, *6*, 9074−9080.
(48) Yue, Y.; Liu, N.; Liu, W.; Li, M.; Ma, Y.; Luo, C.; Wang, S.; Rao, J.; Hu, X.; Su, J.; Zhang, Z.; Huang, Q.; Gao, Y. 3D hybrid porous Mxene-sponge network and its application in piezoresistive sensor. *Nano Energy* **2018**, *50*, 79−87.
(49) Zhao, X.-H.; Ma, S.-N.; Long, H.; Yuan, H.; Tang, C. Y.; Cheng, P. K.; Tsang, Y. H. Multifunctional Sensor Based on Porous Carbon Derived from Metal-Organic Frameworks for Real Time Health Monitoring. *ACS Appl. Mater. Interfaces* **2018**, *10*, 3986−3993.
(50) Mu, C.; Song, Y.; Huang, W.; Ran, A.; Sun, R.; Xie, W.; Zhang, H. Flexible Normal-Tangential Force Sensor with Opposite Resistance Responding for Highly Sensitive Artificial Skin. *Adv. Funct. Mater.* **2018**, *28*, 1707503.
(51) Chun, K.-Y.; Son, Y. J.; Jeon, E.-S.; Lee, S.; Han, C.-S. A Self-Powered Sensor Mimicking Slow- and Fast-Adapting Cutaneous Mechanoreceptors. *Adv. Mater.* **2018**, *30*, 1706299.
(52) Pang, C.; Koo, J. H.; Nguyen, A.; Caves, J. M.; Kim, M.-G.; Chortos, A.; Kim, K.; Wang, P. J.; Tok, J. B.-H.; Bao, Z. Highly Skin-Conformal Microhairy Sensor for Pulse Signal Amplification. *Adv. Mater.* **2015**, *27*, 634−640.
(53) Li, Y.; Hong, L.; Chen, Y.; Wang, H.; Lu, X.; Yang, M. Poly(4-vinylpyridine)/carbon black composite as a humidity sensor. *Sens. Actuators, B* **2007**, *123*, 554−559.
(54) Chen, S. G.; Hu, J. W.; Zhang, M. Q.; Li, M. W.; Rong, M. Z. Gas sensitivity of carbon black/waterborne polyurethane composites. *Carbon* **2004**, *42*, 645−651.

https://dx.doi.org/10.1021/acsami.0c03326
ACS Appl. Mater. Interfaces 2020, 12, 26137−26144